

## Observation of hybrid-order topological pump in a Kekulé-textured graphene lattice

Tianzhi Xia,<sup>1</sup> Yuzeng Li,<sup>1,\*</sup> Qicheng Zhang,<sup>1</sup> Xiying Fan,<sup>1</sup> Meng Xiao<sup>1,2</sup> and Chunyin Qiu<sup>1,†</sup>

<sup>1</sup>*School of Physics and Technology, Wuhan University, Wuhan 430072, China*

<sup>2</sup>*Wuhan Institute of Quantum Technology, Wuhan 430206, China*



(Received 28 July 2023; accepted 7 September 2023; published 18 September 2023)

The Thouless charge pumping protocol provides an effective route for realizing topological particle transport. To date, the first-order and higher-order topological pumps, exhibiting transitions of edge-bulk-edge and corner-bulk-corner states, respectively, are observed in a variety of experimental platforms. Here, we propose the concept of a hybrid-order topological pump that involves a transition of bulk, edge, and corner states simultaneously. More specifically, we consider a Kekulé-textured graphene lattice that features a tunable phase parameter. The finite sample of zigzag boundaries, where the corner configuration is abnormal and inaccessible by repeating unit cells, hosts topological responses at both the edges and corners. The former is protected by a nonzero winding number, while the latter can be explained by a nontrivial vector Chern number. Using our skillful acoustic experiments, we verify these nontrivial boundary landmarks and visualize the consequent hybrid-order topological pump process directly. This work deepens our understanding of higher-order topological phases and broadens the scope of topological pumps.

DOI: [10.1103/PhysRevB.108.125125](https://doi.org/10.1103/PhysRevB.108.125125)

### I. INTRODUCTION

Topology, originally a branch of mathematics, has become an important concept in different fields of physics [1–6]. The Thouless pump provides one of the simplest manifestations to understand band topology in quantum systems. It was first proposed by Thouless when he studied particle transport in one-dimensional (1D) periodic structures with adiabatic time evolution. He found that dynamic edge-bulk-edge pumping shares the same topological origin as the static two-dimensional (2D) Chern insulator [7,8], where one of the momentum coordinates is replaced by an adiabatically varied cyclic parameter [Fig. 1(a)]. As such, this dynamic pumping process can be dictated by a nontrivial integer topological invariant (i.e., the first Chern number). A similar theory has also been extended to explore the four-dimensional (4D) quantum Hall effect characterized by a 4D topological invariant (known as the second Chern number) [9,10]. In this case, a 2D Thouless pump is implemented in a 2D spatial system, resorting to two additional external parameters [10]. With the discovery of higher-order topological insulators [11–15], referring to  $d$ -dimensional topological systems hosting nontrivial  $(d-N)$ -dimensional boundary states ( $N > 1$ ), higher-order topological pumps have been proposed to connect the quantized corner-to-corner charge flow with the unconventional bulk-boundary correspondence [16–21], as illustrated in Fig. 1(b). To date, both the conventional (first-order) and higher-order Thouless pumps have been realized in diverse experimental platforms, from cold atom systems to various artificial crystals of classical waves [22–32].

Note that both the first-order and higher-order pumping procedures involve only a simple transition between the bulk

and edge (or corner) states. To the best of our knowledge, thus far there is no realization of a topological pump involving the states of more spatial dimensions simultaneously, e.g., the bulk, edge, and corner states in a 2D system. To achieve these new types of topological pump, later dubbed hybrid order pumps, a suitable bandgap formed *between* the 2D bulk and the 1D edge bands should be designed in order to tolerate continuous pumping of the zero-dimensional (0D) corner states [Fig. 1(c)]. This is much more difficult than that demanded for a higher-order pump. The validity of the higher-order topological invariant relies on a concrete selection of the periodic unit cell [11–15], which makes the boundary morphology and thus the edge modes predetermined by the corner configuration in the finite system formed by repeating unit cells.

In this work, we report an experimental observation of a hybrid-order topological pump in an acoustic system. As shown in Fig. 2(a), we consider a 2D Kekulé-textured graphene (KTG) lattice featuring three inequivalent hoppings, where the variable phase ( $\phi$ ) acts as the cyclic pumping parameter. In particular, we focus on the obtuse angle corners intersected by two zigzag boundaries. In this unusual boundary configuration, which is inaccessible by repeating any minimal unit cells, the system exhibits corner states that traverse the edge and bulk states continuously with the phase parameter. Using acoustic cavity tube structures, we experimentally observe the highly appealing hybrid-order topological pumping process accompanying convincing experimental evidence for the topological responses at the 1D edges and 0D corners.

### II. TIGHT-BINDING MODEL

As shown in Fig. 2(a), we start with a 2D KTG model that is distorted from the graphene lattice of uniform

\*yuzengli@whu.edu.cn

†cyqiu@whu.edu.cn

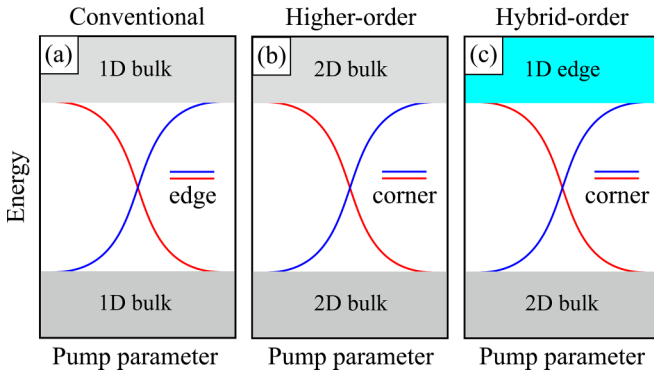


FIG. 1. Schematic illustrations for three distinct topological pumps. (a) Conventional (first-order) pump in 1D systems. (b) Higher-order topological pump in 2D systems. (c) Hybrid-order topological pump in 2D systems. The red and blue lines sketch 0D states confined to different edges (or corners). In contrast to conventional and higher-order pumps that exhibit edge-bulk-edge and corner-bulk-corner transports within a parameter cycle, the hybrid-order pump exhibits a transition among the bulk, edge, and corner states.

hopping  $t_0$  [33,34]. The KTG lattice features three inequivalent nearest-neighboring hoppings  $t_n = t_0 + \delta t \cos(\chi_n + \phi)$ , where  $\delta t$  characterizes the modulation strength of the hoppings, and  $\phi \in [-\pi, \pi]$  is a tunable phase parameter under the specific bias  $\chi_n = 2(n-1)\pi/3$  ( $n = 1 \sim 3$ ). Note that the lattice constant  $a$  of the honeycomb lattice becomes  $\sqrt{3}a$  for the KTG lattice. In addition to time-reversal symmetry, the system with a general  $\phi$  has sublattice symmetry (or chiral symmetry). It is of particular interest that, as exhibited in Fig. 2(b), the band structure of the KTG lattice always hosts a wide spectral gap centered at zero energy, in addition to the minigaps appearing repeatedly between the highest (lowest) two bands.

Now we consider the topological boundary manifestations in finite-sized samples. Armchair and zigzag boundaries are two typical boundary truncations for general honeycomb lattices. In our KTG lattice, however, unlike the armchair boundary accessible by simply duplicating unit cells, the zigzag boundary cannot be achieved without destroying the integrity of the six-orbital KTG unit cell. Instead, it can be realized by repeating rhombus supercells of 18 orbitals. Figure 2(c) presents the spectral flow against the phase parameter  $\phi$  for the case of the natural armchair boundary. It shows that near  $\phi = 0$ , two degenerate zero-energy states emerge at the corners of the obtuse angle, either symmetric or antisymmetric about the center of the finite diamond-shaped structure. The corner states can be explained by a  $Z_2$  topological invariant or a topological index defined at the high symmetry points in momentum space [34–37]. For the system with the unusual zigzag boundary, however, novel phenomena emerge in the primary bulk gap. As shown in Fig. 2(d), highly degenerate flat bands (cyan curves) appear at zero energy and divide the primary gap into two pieces. These are edge states inherited from the original graphene lattice of the zigzag boundary, which can be characterized by a nontrivial winding number [38,39] (see Fig. S1 in Supplemental Material [40]). More intriguingly, there are two sets of corner states spanning the two

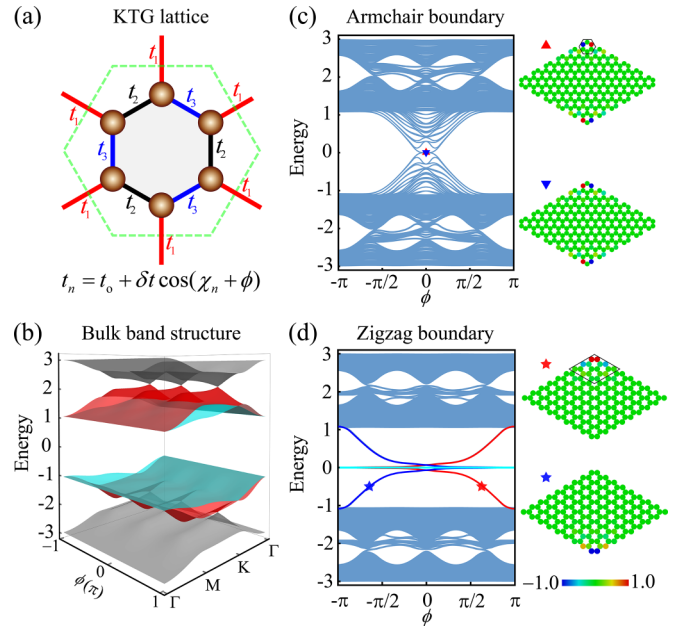


FIG. 2. Tight-binding model. (a) Unit cell of the KTG lattice, which features textured hoppings  $t_1$ ,  $t_2$ , and  $t_3$ . (b) Evolution of the band structure as the phase parameter  $\phi$ , evaluated with fixed  $t_0 = -1$  and  $\delta t = -0.7$ . (c) Left:  $\phi$ -Dependent energy spectrum for a finite system with an armchair boundary. Right: Eigenfields for the degenerate zero-energy corner states highlighted in the spectrum. (d) Similar to (c), but for the system with a zigzag boundary. Note that the corner configuration cannot be formed by simply repeating KTG unit cells or any other minimal unit cells of six orbitals, but it can be achieved by duplicating the rhombus supercell of 18 orbitals. The coexistence of the nontrivial edge (cyan) and corner (red and blue) modes offers an opportunity to realize a hybrid-order topological pumping in the zigzag-boundary KTG lattice.

separate primary gaps with the continuum evolution of  $\phi$ , each of which emerges pairwise in energy at the same corner due to the chiral symmetry. In addition, the corner states associated with the samples of  $\pm\phi$  are localized in opposite obtuse-angle corners, as exemplified by the field distributions for  $\phi = \pm 5\pi/8$ . Therefore, for any of the two divided primary gaps, one can imagine a hybrid-order topological pumping process that involves the bulk, edge, and corner states simultaneously.

### III. TOPOLOGICAL NATURE OF THE GAPLESS CORNER STATES

Knowing that the edge states are protected by a nontrivial winding number, we next explain the physical origin for the gapless corner states in the zigzag-boundary systems, inspired by the top-to-bottom scheme introduced in Ref. [41], from which one constructs 2D corner states from two independent 1D systems with 0D edge states. To do this, we consider a finite system of  $N \times N$  rhombus supercells and decompose it into  $N$  1D supercell chains in the  $a$  and  $b$  directions [Fig. 3(a)]. Each supercell chain constitutes a 2D Chern insulator when introducing the phase parameter  $\phi$  as an effective momentum for the second, synthetic dimension. Figure 3(b) shows the bulk band structure for the synthetic 2D Chern insulator, where the chiral symmetry-related bands are plotted with the

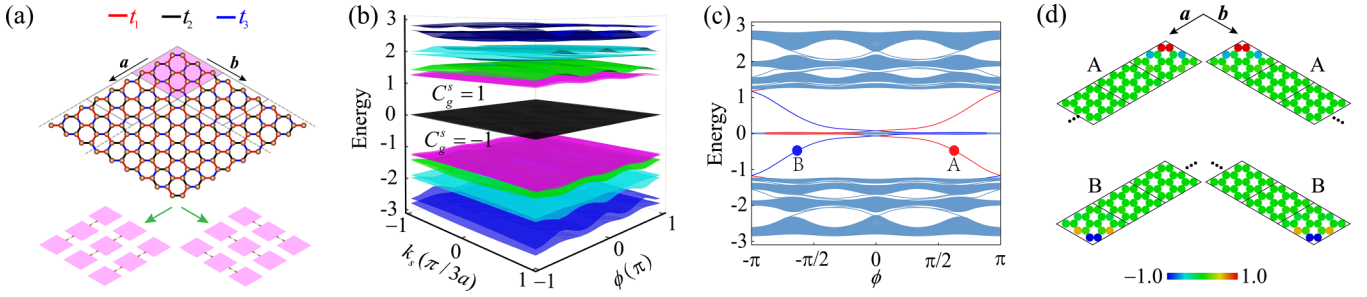


FIG. 3. Physical origin of the gapless corner states. (a) A zigzag-boundary KTG lattice formed by duplicating rhombus supercells (shaded). It can be decoupled into supercell chains along the  $a$  and  $b$  directions by removing the inter-supercell hoppings in the  $b$  and  $a$  directions, respectively. (b) Global evolution of the band structure for the 1D periodic chain in the  $a(b)$  direction, which emulates the bulk dispersion of a 2D Chern insulator under the assistance of the effective momentum  $\phi$ . Here,  $C_g^s$  highlights the Chern number for the two primary gaps near the zero-energy flat bands. (c)  $\phi$ -Dependent energy spectrum for the  $a(b)$ -directed chain of finite length, which exhibits in-gap edge modes (blue and red lines) protected by the gap Chern numbers. (d) Field distributions of the edge modes labeled in (c), which together form the top (A) and bottom (B) corner modes in Fig. 2(d).

same color for clarity. In particular, the two nearly degenerate flat bands (black) share a similar physical origin to those edge modes exhibited in Fig. 2(d), while the states are now localized at the *supercell's* zigzag boundaries. According to the bulk-boundary correspondence, the topological edge states of the synthetic Chern insulator are related to its gap Chern number, which can be defined as

$$C_g^s = \frac{1}{2\pi i} \int_{\text{BZ}} \text{Tr}[F(k_s, \phi)] dk_s d\phi. \quad (1)$$

Here,  $s = a, b$  and  $F(k_s, \phi)$  represents the non-Abelian Berry curvature calculated for all bands below the target gap [41,42]. Specifically, the gap Chern number  $C_g^s = 1$  ( $-1$ ) for the primary gap above (below) the flat bands. This suggests that each gap hosts one gapless edge band when the synthetic Chern insulator is truncated in the  $a(b)$  direction. This can be seen in Fig. 3(c), which shows the projected energy spectrum along the synthetic momentum  $\phi$ . Figure 3(d) exemplifies the edge-state distributions for  $\phi = \pm 5\pi/8$  in the lower primary gap. When both the  $a$ - and  $b$ -directed supercell chains host nontrivial edge states decaying exponentially away from the ends, corner states are concluded in the 2D zigzag-boundary sample whose couplings can be decomposed into two independent components in these directions [41,42]. (More specifically, the top edge localizations in  $\phi = 5\pi/8$  contribute the top corner states, while the bottom edge localizations for  $\phi = -5\pi/8$  contribute the bottom corner states [Fig. 2(d)].) Therefore, the corner states of the original zigzag-boundary KTG lattice can be characterized by the two nonzero-gap Chern numbers  $C_g^a$  and  $C_g^b$ , or written together as a vector,  $\mathbf{C} = (C_g^a, C_g^b)$ . More specifically, the vector Chern numbers  $C_1 = (-1, -1)$  and  $C_2 = (1, 1)$  explain the corner states of the primary gaps below and above the zero energy, respectively. Ultimately, the coexistence of the topological corner and edge states in the diamond-shaped sample, protected respectively by the nontrivial vector Chern numbers and the winding numbers, enables a unique hybrid-order pumping process when considering a continuous evolution of the phase parameter  $\phi$ .

#### IV. ACOUSTIC REALIZATION OF THE TIGHT-BINDING MODEL

The previous tight-binding model can be emulated precisely by our acoustic system, where the orbitals and hoppings are mimicked by air-filled cavity resonators and narrow tubes [43–46], respectively. As shown in Fig. 4(a), each unit cell of our acoustic KTG lattice includes six identical hexagonal prism cavities of side length  $l = 5.0$  mm and height  $H = 32.8$  mm. The latter results in a dipole resonant mode of 5.27 kHz, which is far from the other resonant modes. (In our simulations, the sound speed is set as 346 m/s.) Every two nearest acoustic resonators are connected by two rectangular tubes with a constant aspect ratio 1 : 3. Provided that the couplings are approximately proportional to the cross-sectional areas of the narrow tubes, as shown in Fig. 4(b), we realize the desired couplings by modulating the cross-sectional areas  $S_n = S_0 + \delta S \cos(\chi_n + \phi)$ , with  $S_0 = 20.3$  mm<sup>2</sup> and  $\delta S = 12.0$  mm<sup>2</sup>. The resultant effective hoppings (colored dots) capture well the cosine line shape  $t_n = t_0 + \delta t \cos(\chi_n + \phi)$ , associated with  $t = -424.5$  Hz and  $\delta t = -216.7$  Hz. To demonstrate the topological response of the system, Fig. 4(c) exemplifies the eigenvalue spectrum with  $\phi = 5\pi/8$ , simulated for a sample of  $3 \times 3$  supercells. In addition to the midgap edge modes, the energy spectrum features two chiral symmetry-related 0D modes at the top corner of the sample, as visualized further by their acoustic field distributions (see insets).

Here we present our experimental evidence for the topological edge and corner states. We focus on the sample with  $\phi = 5\pi/8$  first. As shown in Fig. 4(d), our sample fabricated by three-dimensional printing consists of  $3 \times 3$  supercells, i.e., 162 acoustic cavity resonators in total. To implement local measurements, two small holes are perforated in each cavity for inserting the sound source and probe, which are sealed when not in use. Both the input and output signals are recorded and frequency-resolved with a multianalyzer system (B&K Type 4182). The samples are divided into nonoverlapping spatial domains to extract the information of the bulk, edge, and corner states. The top panel of Fig. 4(e) presents the site-averaged bulk, edge, and corner spectra. Clearly, the bulk spectrum (gray curve) shows a wide bandgap centered at

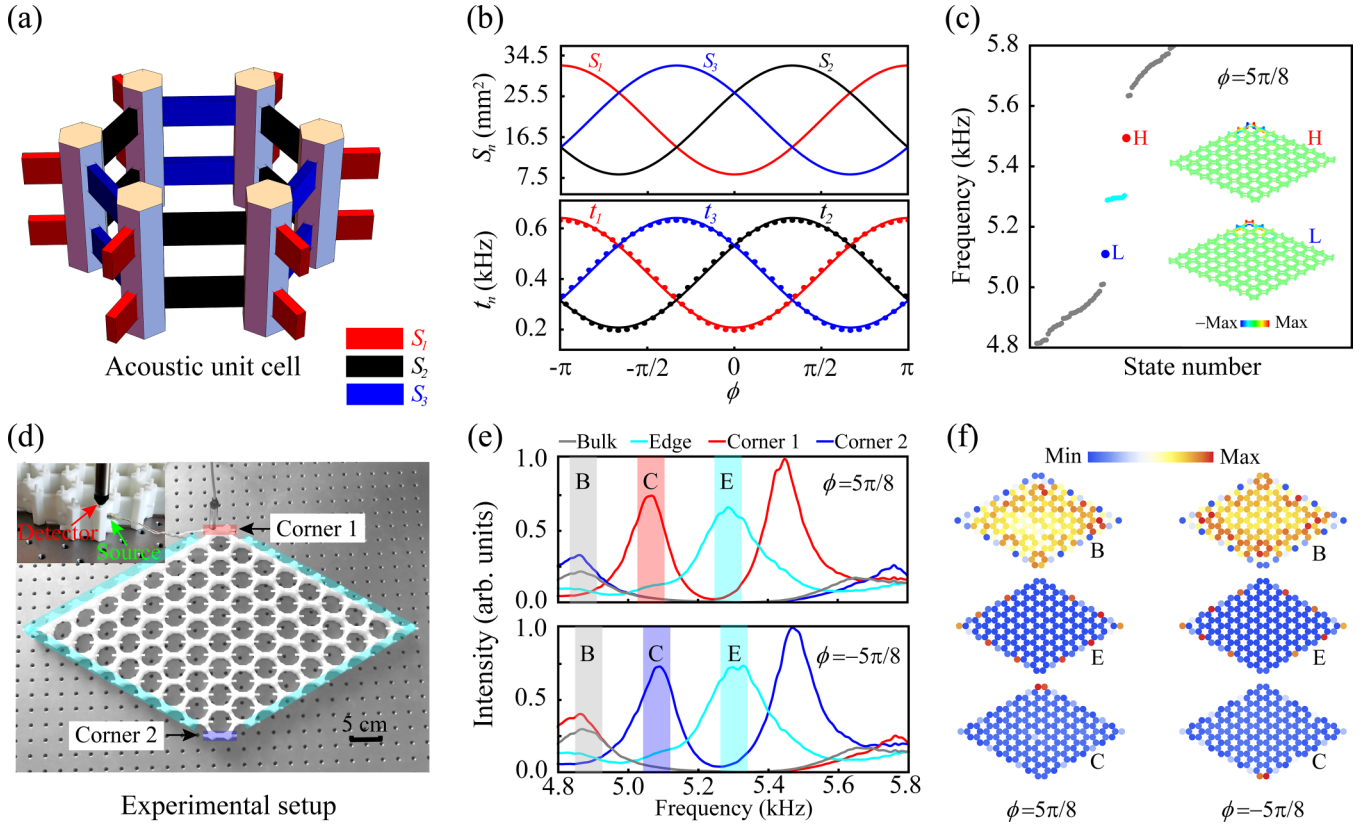


FIG. 4. Acoustic emulation of the tight-binding model and experimental evidence for the topological states. (a) Unit cell geometry of our acoustic KTG lattice, which features three types of coupling tubes of different cross-sectional areas:  $S_1$ ,  $S_2$ , and  $S_3$ . (b) Top:  $\Phi$ -Dependent cross-sectional areas designed for the three coupling tubes. Bottom: Associated effective couplings (colored dots), which are fitted well by cosine functions (colored lines). (c) Eigenfrequency spectra simulated for a finite sample with  $\phi = 5\pi/8$ . Insets: Pressure field distributions extracted for the two chiral symmetry-related corner states. (d) A photograph of the zigzag-boundary sample, where the corner and edge sites are colored for clarity. The inset shows an enlarged view around corner 1. (e) Pressure intensity spectra averaged for the bulk (B), edge (E), and corner (C) sites. The results are exemplified with the samples of  $\phi = \pm 5\pi/8$ . (f) Intensity patterns extracted for the bulk, edge, and corner states, which are averaged over the frequency windows shadowed in (e).

5.27 kHz (associated with the zero energy in the tight-binding model), around which the edge spectrum (cyan curve) shows a predominant peak. By contrast, a pair of chiral symmetry-related peaks appear in the spectrum of corner 1 (red curve), which are missed in the spectrum of corner 2 (blue curve), as predicted in Fig. 2(d). Similar phenomena can be observed in the case of  $\phi = -5\pi/8$  [Fig. 4(e), bottom panel], where the corner states appear in corner 2 (blue curve). To identify the bulk, edge, and corner states further, we have integrated the pressure intensities over several typical frequency ranges for each site individually. As shown in Fig. 4(f), the site-resolved acoustic patterns exhibit clear spatial characteristics of the bulk, edge, and corner states as expected. It is worth pointing out that in graphene-like lattices, although extensively unveiled in armchair-boundary configurations, the higher-order corner states have not been observed so far in any system with zigzag boundaries.

## V. OBSERVATION OF THE HYBRID-ORDER TOPOLOGICAL PUMP

To reflect the global evolution of the bulk, edge, and corner states within one pumping cycle  $\phi \in [-\pi, \pi]$ , we

fabricated 17 diamond-shaped samples at the  $\phi$ -step of  $\pi/8$  and measured their topological manifestations individually as before. All experimental data match well with our full-wave simulated bulk, edge, and corner spectra (see Fig. S2 in Supplemental Material [40]). For conciseness, here we count the bulk, edge, and corner spectra together and present the superimposed data (color scale) in Fig. 5(a). It exhibits an excellent agreement with our theoretical prediction (colored lines), especially for the corner modes across the two primary bandgaps around 5.3 kHz. The band broadening stems mostly from the unavoidable viscous and thermal dissipations inside the acoustic structure. More importantly, the spectral flow unveils a hybrid-order topological pumping process where the corner states traverse the bulk and edge states smoothly, as guided by the white arrows in the lower primary gap. To visualize the intricate hybrid-order topological pump directly, we display the site-resolved intensity patterns measured for a set of typical configurations [Fig. 5(b), left]. Clearly, the acoustic state evolves from the top corner 1 to the bulk 2, consequently to the bottom corner 3, and then it goes back to the initial state 5 through the edge 4, during which the bandgap is never closed. This reproduces the pumping process predicted by the tight-binding model [Fig. 5(b), right].

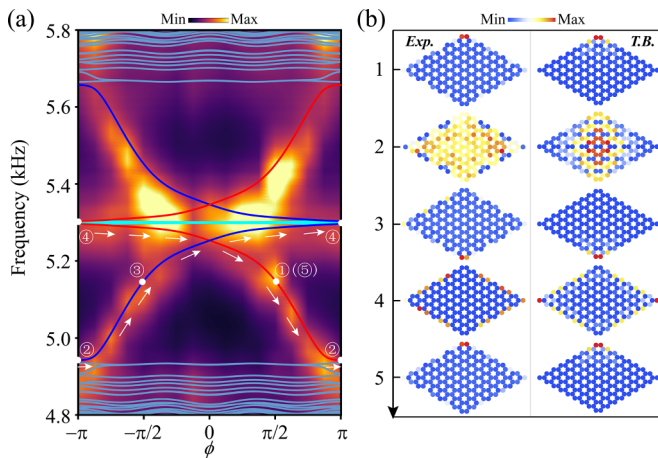


FIG. 5. Experimental observation of the hybrid-order topological pump. (a) Global evolution of the bulk, edge, and corner spectra (color scale), together with the tight-binding predictions (colored lines) for comparison. The white arrows highlight an intact pumping process. (b) Field distributions scanned for the states labeled from 1 to 5, compared with the tight-binding results. The data exhibit a clear hybrid-order topological pump that involves the corner, bulk, and edge states simultaneously.

## VI. CONCLUSION

By fully exploiting the controllability of acoustic metamaterials, we have designed and fabricated a series of acoustic KTG lattices to realize a novel hybrid-order topological pumping protocol. Tracking the global evolution of the acoustic states with the cyclic parameter, our experimental results exhibit an intact corner-bulk-corner-edge-corner transition, which involves the 0D corner, 1D edge, and 2D bulk states simultaneously. All experimental data agree well with the theoretical predictions. One may expect that both the corner states and edge states involved here would be considerably robust against disorders and defects, given the protection by the gap Chern and winding numbers. Our findings open a new path for unveiling more complex topological pumping physics.

## ACKNOWLEDGMENTS

This project was supported by the National Natural Science Foundation of China (Grants No. 11890701, No. 12374418, No. 12004287, and No. 12104346) and the Young Top-Notch Talent for Ten Thousand Talent Program (2019–2022).

- [1] K. V. Klitzing, The quantized Hall effect, *Rev. Mod. Phys.* **58**, 519 (1986).
- [2] C. L. Kane and Liang Fu, Time reversal polarization and a  $Z_2$  adiabatic spin pump, *Phys. Rev. B* **74**, 195312 (2006).
- [3] X. Qi, T. L. Hughes, and S. Zhang, Topological field theory of time-reversal invariant insulators, *Phys. Rev. B* **78**, 195424 (2008).
- [4] X. Qi, T. L. Hughes, S. Raghu, and S. Zhang, Time-Reversal-Invariant Topological Superconductors and Superfluids in Two and Three Dimensions, *Phys. Rev. Lett.* **102**, 187001 (2009).
- [5] M. Z. Hasan and C. L. Kane, Colloquium: Topological insulators, *Rev. Mod. Phys.* **82**, 3045 (2010).
- [6] X. Qi and S. Zhang, Topological insulators and superconductors, *Rev. Mod. Phys.* **83**, 1057 (2011).
- [7] D. J. Thouless, Quantization of particle transport, *Phys. Rev. B* **27**, 6083 (1983).
- [8] R. Citro and M. Aidelsburger, Thouless pumping and topology, *Nat. Rev. Phys.* **5**, 87 (2023).
- [9] S.-C. Zhang and J. Hu, A four-dimensional generalization of the quantum Hall effect, *Science* **294**, 823 (2001).
- [10] Y. E. Kraus, Z. Ringel, and O. Zilberberg, Four-Dimensional Quantum Hall Effect in a Two-Dimensional Quasicrystal, *Phys. Rev. Lett.* **111**, 226401 (2013).
- [11] W. A. Benalcazar, B. A. Bernevig, and T. L. Hughes, Quantized electric multipole insulators, *Science* **357**, 61 (2017).
- [12] W. A. Benalcazar, B. A. Bernevig, and T. L. Hughes, Electric multipole moments, topological multipole moment pumping, and chiral hinge states in crystalline insulators, *Phys. Rev. B* **96**, 245115 (2017).
- [13] Z. Song, Z. Fang, and C. Fang, ( $d-2$ )-Dimensional Edge States of Rotation Symmetry Protected Topological States, *Phys. Rev. Lett.* **119**, 246402 (2017).
- [14] F. Schindler, A. M. Cook, M. G. Vergniory, Z. Wang, S. S. P. Parkin, B. A. Bernevig, and T. Neupert, Higher-order topological insulators, *Sci. Adv.* **4**, eaat0346 (2018).
- [15] F. Schindler, Z. Wang, M. G. Vergniory, A. M. Cook, A. Murani, S. Sengupta, A. Y. Kasumov, R. Deblock, S. Jeon, I. Drozdov, H. Bouchiat, S. Guéron, A. Yazdani, B. A. Bernevig, and T. Neupert, Higher-order topology in bismuth, *Nat. Phys.* **14**, 918 (2018).
- [16] B. Kang, W. Lee, and G. Y. Cho, Many-Body Invariants for Chern and Chiral Hinge Insulators, *Phys. Rev. Lett.* **126**, 016402 (2021).
- [17] J. F. Wienand, F. Horn, M. Aidelsburger, J. Bibo, and F. Grusdt, Thouless Pumps and Bulk-Boundary Correspondence in Higher-Order Symmetry-Protected Topological Phases, *Phys. Rev. Lett.* **128**, 246602 (2022).
- [18] I. Petrides and O. Zilberberg, Higher-order topological insulators, topological pumps and the quantum Hall effect in high dimensions, *Phys. Rev. Res.* **2**, 022049(R) (2020).
- [19] B. Y. Xie, O. B. You, and S. Zhang, Photonic topological pump between chiral disclination states, *Phys. Rev. A* **106**, L021502 (2022).
- [20] B. L. Wu, A. M. Guo, Z. Q. Zhang, and H. Jiang, Quantized charge-pumping in higher-order topological insulators, *Phys. Rev. B* **106**, 165401 (2022).
- [21] Y. P. Wu, L. Z. Tang, G. Q. Zhang, and D. W. Zhang, Quantized topological Anderson-Thouless pump, *Phys. Rev. A* **106**, L051301 (2022).
- [22] Y. E. Kraus, Y. Lahini, Z. Ringel, M. Verbin, and O. Zilberberg, Topological States and Adiabatic Pumping in Quasicrystals, *Phys. Rev. Lett.* **109**, 106402 (2012).
- [23] S. Nakajima, T. Tomita, S. Taie, T. Ichinose, H. Ozawa, L. Wang, M. Troyer, and Y. Takahashi, Topological Thouless pumping of ultracold fermions, *Nat. Phys.* **12**, 296 (2016).

- [24] M. Lohse, C. Schweizer, O. Zilberberg, M. Aidelsburger, and I. Bloch, A Thouless quantum pump with ultracold bosonic atoms in an optical superlattice, *Nat. Phys.* **12**, 350 (2016).
- [25] O. Zilberberg, S. Huang, J. Guglielmon, M. Wang, K. P. Chen, Y. E. Kraus, and M. C. Rechtsman, Photonic topological boundary pumping as a probe of 4D quantum Hall physics, *Nature (London)* **553**, 59 (2018).
- [26] M. Lohse, C. Schweizer, H. M. Price, O. Zilberberg, and I. Bloch, Exploring 4D quantum Hall physics with a 2D topological charge pump, *Nature (London)* **553**, 55 (2018).
- [27] W. Chen, E. Prodan, and C. Prodan, Experimental Demonstration of Dynamic Topological Pumping Across Incommensurate Bilayered Acoustic Metamaterials, *Phys. Rev. Lett.* **125**, 224301 (2020).
- [28] I. H. Grinberg, M. Lin, C. Harris, W. A. Benalcazar, C. W. Peterson, T. L. Hughes, and G. Bahl, Robust temporal pumping in a magneto-mechanical topological insulator, *Nat. Commun.* **11**, 974 (2020).
- [29] M. I. N. Rosa, R. K. Pal, J. R. F. Arruda, and M. Ruzzene, Edge States and Topological Pumping in Spatially Modulated Elastic Lattices, *Phys. Rev. Lett.* **123**, 034301 (2019).
- [30] H. Chen, H. Zhang, Q. Wu, Y. Huang, H. Nguyen, E. Prodan, X. Zhou, and G. Huang, Creating synthetic spaces for higher-order topological sound transport, *Nat. Commun.* **12**, 5028 (2021).
- [31] W. A. Benalcazar, J. Noh, M. Wang, S. Huang, K. P. Chen, and M. C. Rechtsman, Higher-order topological pumping and its observation in photonic lattices, *Phys. Rev. B* **105**, 195129 (2022).
- [32] S. Y. Wang, Z. Hu, Q. Wu, H. Chen, E. Prodan, R. Zhu, and G. L. Huang, Smart patterning for topological pumping of elastic surface waves, *Sci. Adv.* **9**, eadh431 (2023).
- [33] C. Y. Hou, C. Chamon, and C. Mudry, Electron Fractionalization in Two-Dimensional Graphenelike Structures, *Phys. Rev. Lett.* **98**, 186809 (2007).
- [34] J. Noh, W. A. Benalcazar, S. Huang, M. J. Collins, K. P. Chen, T. L. Hughes, and M. C. Rechtsman, Topological protection of photonic mid-gap defect modes, *Nat. Photonics* **12**, 408 (2018).
- [35] W. A. Benalcazar, T. Li, and T. L. Hughes, Quantization of fractional corner charge in  $C_n$ -symmetric higher-order topological crystalline insulators, *Phys. Rev. B* **99**, 245151 (2019).
- [36] E. Lee, A. Furusaki, and B. Yang, Fractional charge bound to a vortex in two-dimensional topological crystalline insulators, *Phys. Rev. B* **101**, 241109 (2020).
- [37] H. Qiu, M. Xiao, F. Zhang, and C. Qiu, Higher-Order Dirac Sonic Crystals, *Phys. Rev. Lett.* **127**, 146601 (2021).
- [38] W. Yao, S. A. Yang, and Q. Niu, Edge States in Graphene: From Gapped Flat-Band to Gapless Chiral Modes, *Phys. Rev. Lett.* **102**, 096801 (2009).
- [39] C.-K. Chiu, J. C. Y. Teo, A. P. Schnyder, and S. Ryu, Classification of topological quantum matter with symmetries, *Rev. Mod. Phys.* **88**, 035005 (2016).
- [40] See Supplemental Material at <http://link.aps.org/supplemental/10.1103/PhysRevB.108.125125> for details of the topological origin of the flat edge bands in KTG lattice and the site-averaged spectra belong to the bulk, edge and corner.
- [41] Y. Wang, Y. Ke, Y. Chang, Y. Lu, J. Gao, C. Lee, and X. Jin, Constructing higher-order topological states in higher dimensions, *Phys. Rev. B* **104**, 224303 (2021).
- [42] Z. Chen, W. Zhu, Y. Tan, L. Wang, and G. Ma, Acoustic Realization of a Four-Dimensional Higher-Order Chern Insulator and Boundary-Modes Engineering, *Phys. Rev. X* **11**, 011016 (2021).
- [43] H. Xue, Y. Ge, H.-X. Sun, Q. Wang, D. Jia, Y.-J. Guan, S.-Q. Yuan, Y. Chong, and B. Zhang, Observation of an acoustic octupole topological insulator, *Nat. Commun.* **11**, 2442 (2020).
- [44] X. Ni, M. Li, M. Weiner, A. Alù, and A. B. Khanikaev, Demonstration of a quantized acoustic octupole topological insulator, *Nat. Commun.* **11**, 2108 (2020).
- [45] Y. Qi, C. Qiu, M. Xiao, H. He, M. Ke, and Z. Liu, Acoustic Realization of Quadrupole Topological Insulators, *Phys. Rev. Lett.* **124**, 206601 (2020).
- [46] T. Li, J. Du, Q. Zhang, Y. Li, X. Fan, F. Zhang, and C. Qiu, Acoustic Möbius Insulators from Projective Symmetry, *Phys. Rev. Lett.* **128**, 116803 (2022).